引用格式：LIU Qingmin, HOU Shanglin, LEI Jingli. Design and Analysis of D-shaped Surface Plasmon Resonance Fiber Biosensor for Liquid Analytes[J]. Acta Photonica Sinica, 2022, 51(9):0906007
刘庆敏,侯尚林,雷景丽.D型表面等离子共振光纤液体生物传感器设计与分析[J].光子学报,2022,51(9):0906007

D型表面等离子共振光纤液体生物传感器设计与分析

刘庆敏,侯尚林,雷景丽
(兰州理工大学 理学院, 兰州 730050)

摘 要:为探测在近红外和中红外的低折射率物质,提出一种新型的基于D形开环光子晶体光纤的金表面等离子体共振低折射率传感器,并用有限元方法对该传感器的传感性能进行了分析。结果表明该传感器在波长2 020～3 036 nm范围内可检测1.18～1.30的折射率;在1.23到1.30的低折射率范围内,该传感器的光谱灵敏度平均值为11 650 nm/RIU;当折射率在1.29到1.30之间变化时,光谱灵敏度和分辨率可分别达到最大值38 800 nm/RIU和2.37×10^{-6} RIU。该传感器可实现近红外和中红外波段的低折射率检测,在生物医学传感、水环境及湿度检测等领域具有潜在的应用前景。

关键词:光纤传感;表面等离子共振;有限元法;光子晶体光纤;低折射率传感器
中图分类号:TN29 **文献标识码**:A **doi**:10.3788/gzxb20225109.0906007

0 Introduction

Surface Plasmon Resonance (SPR) is a prominent optical phenomenon that arises as to the extent of energy transferring from photons to surface plasmon waves under appropriate conditions[1]. In the past few years, this optical effect, owing to its high sensitivity, real-time detection, and anti-interference, has already been extensively investigated and applied in the fields of medical treatment[2], environment monitoring[3], biomedical sensing[4] and so on. The earliest SPR sensing devices were based on prism[5], such as the Kretschmann-Raether prism[6], whose sensitivity reached up to 10^{-6} RIU. Even though the prism can achieve high sensitivity, it has the disadvantage of costly integration, limited mechanical reliability and difficulties in mass production, which were limited to use in remote monitoring. Optical fiber-based SPR sensors have been exploited in recent years due to their advantages of easy miniaturization, low manufacturing cost and in-situ monitoring[7], etc. Especially, the sensors based on Photonic Crystal Fiber (PCF) can be easy phase-matching and encapsulation because of the minimized size, tunable geometric parameters and flexible design[8], so it becomes a promising candidate for assembling compact and ultra-sensitive SPR sensors with fast, sustainable and real-time monitoring.

As is well known that the sensing performance of Photonic Crystal Fiber-surface Plasmon Resonance (PCF-SPR) sensors depends on the metallic materials and the structure of PCF. Among the various plasmonic materials, gold[9] and silver[10] are mostly used due to their relatively low loss in the visible and near-infrared region, which makes it more effective to monitor the high energy transfer on the surface of plasmonic materials. To date, much effort has been devoted to the structure design of PCF to enhance the sensing performance of

Foundation item: National Natural Science Foundation of China (No. 61665005), HongLiu First-class Disciplines Development Program of Lanzhou University of Technology
First author: LIU Qingmin (1991-), female, M. S. degree candidate, mainly focuses on optical fiber communication and sensing technology. Email:celina1026@163.com
Supervisor (Contact author): HOU Shanglin (1970-), male, professor, Ph.D. degree, mainly focuses on optical fiber communication and sensing technology. Email:houshanglin@vip.163.com
Received: Feb.8,2022; **Accepted**: May 26,2022

PCF-SPR sensors[11], and considerable variety of PCF-SPR structures have been reported, which can be divided into two categories, internal metal-coated structures using selectively coating or nanowires filled, and external metal-coated structures such as D-shaped, slotted and exposed core PCFs[12]. Among them, D-shaped PCF has attracted many interests compared with other PCF structures, because it can not only provide a good solution to the difficulties in a uniform coating which means the precise control of the thickness and roughness of the metal film on the outer surface of the optical fiber, but also solve the problem of filling analytes to Nano-size holes[13]. For example, AN Guowen, et al[14] proposed a D-shaped PCF-SPR sensor with a triangular lattice and four large-size channels, which can obtain the maximum wavelength sensitivity of 10 493 nm/RIU at 1.38. SINGH S and PRAJAPATI Y[15] presented a D-shape PCF-SPR sensor with gold-graphene layers on the surface. The sensitivity is 33 500 nm/RIU and the effective RI resolution is as high as 2.98×10^{-5} RIU for analyte RIs between 1.32 and 1.40. It can be seen from these reported literatures that the most reported D-shaped SPR sensors exhibit good sensing performance when the Refractive Index (RI) of the analyte is higher than 1.30.

However, with the development of biomedicine and material chemistry, the detection for low refractive index analyte has been paid more attention. For example, the RI of sevoflurane in the drug is around 1.27[16], the refractive index of some fluorine-containing organics compounds in water pollution is about 1.30[17]. Hence, it is essential for us to exploit sensors with high sensitivity for detecting low RI. In recent years, some research work about the RI of analytes lower than 1.30 has been conducted. For example, WANG Famei et al[18] studied a D-shaped sensor with two parallel to detect low RI ranging from 1.27 to 1.32 with the maximum spectral sensitivity up to 13 500 nm/RIU and the resonance wavelength ranging between 720 nm and 1 680 nm. LIU Chao et al[19] reported a mid-infrared PCF-SPR sensor with RI detection range of 1.23～1.29 and average sensitivity of 5 500 nm/RIU. CHEN Xin et al[20] proposed a D-type PCF-SPR sensor which operates in the mid-infrared band from ranging 2 530 nm to 2 750 nm with RI of 1.26～1.29 and the maximum sensitivity of 11 055 nm/RIU. In most of these studies, the reports of PCF-SPR sensor with operating wavelength in mid-infrared range are relatively few. In fact, SPR sensors operating in the mid-infrared wavelength have unique advantages compared to the visible and near-infrared bands[21]. For example, it is conducive to improve the detection accuracy and sensitivity of the sensor to large samples as living cells[22], and avoid the light damage to the biological samples[23]. Therefore, it is necessary to exploit the PCF-SPR sensor with higher sensitivity in mid-infrared waveband.

Herein, a novel D-shaped PCF-SPR sensor for detecting low RI analytes is proposed and analyzed. The open-ring channel coated with gold film can not only reduce the coating area, but also simplify the fabrication process. Numerical results show that a maximum spectral sensitivity of 38 800 nm/RIU can be obtained when analyte RI is 1.30 with a high resolution of 2.37×10^{-6}RIU. The operating wavelength of this fiber sensor includes the near- and mid-infrared regions ranging from 2 020 nm to 3 036 nm. This proposed sensor is of significance in environmental engineering, biosensors and healthcare.

1 Design and analysis of the model

The cross-section of the proposed D-shaped SPR sensor is illustrated in Fig. 1. This structure contains three layers of air rings. The radii of air holes in the first-layer and third-layer are r_1 and r_3, respectively. While the second-layer air ring consists of air holes with two different radii, r_2 and r_s. The refractive index of air is fixed at $n_{air}=1$ and the radius of the cladding is R. A thin gold film with thickness t_g is deposited on the inner surface of the micro-opening analyte channel on the upper side, the radius and the center location of the channel are r_s and $2.5\times\Lambda-1.25\times r_s$, respectively. The first layer of air holes is composed of regular octagonal air holes with a radius of r_1 and a distance of Λ from the fiber core, the second layer of air holes consists of a large air hole with radius of r_s and ten small air holes with radius of r_2. The large air hole is located directly below the fiber core and the distance from the fiber core is $2.5\times\Lambda-1.25\times r_s$, while the small air holes with radius of r_2 are arranged in two ways. One is distributed on both sides of the large air hole and the distance from the fiber core is $2.5\times\Lambda-1.25\times r_s$, it is composed of four air holes with a radius of r_2 which are 30 degrees from the vertical center line. The remaining six air holes are left-right symmetrical structure, in which the abscissa of the three air

holes on the right is $\sqrt{3}\,\Lambda$, the distance between the three adjacent air holes on the right is Λ, and the remaining three air holes on the left are symmetrically distributed with the three air holes on the right. The outermost air holes are obtained by rotating the air holes with a radius of r_3 with an abscissa of 2.5Λ and an ordinate of 0.5Λ for three times, and each rotation angle is 30°. Then four air holes will be obtained with a radius of r_3, while the four air holes in the outermost layer on the left are symmetrically distributed with the four air holes with a radius of r_3 on the right. The air hole structure of the proposed sensor is symmetrical so as to enlarge the energy leakage from the fiber core to enhance the coupling between optical and plasmonic modes.

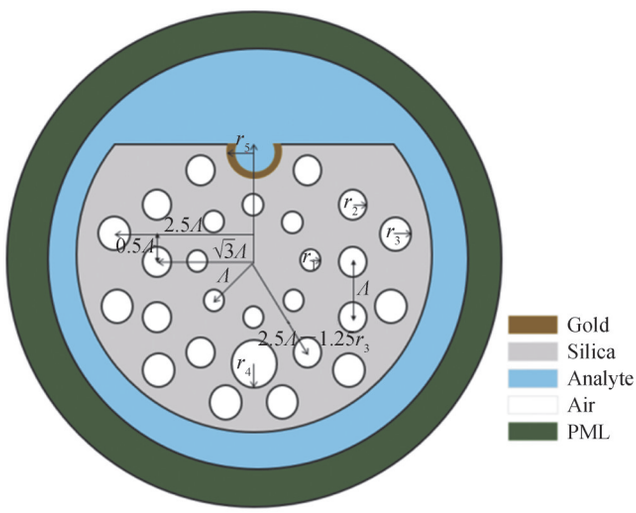

Fig. 1 Schematic illustration of the proposed D-shaped PCF-sensor

The D-shaped sensors can be fabricated by stack-and-draw method[24] and side-polishing technique[25], the gold film can be coated on the inner surface of the micro-opening channel by chemical vapor method[26]. The fiber material is fused silica and the RI is determined by the Sellmeier equation[27]

$$n^2-1=\frac{0.6961663\lambda^2}{\lambda^2-0.0684043^2}+\frac{0.4079426\lambda^2}{\lambda^2-0.1162414^2}+\frac{0.897479\lambda^2}{\lambda^2-9.896161^2} \tag{1}$$

where λ represents the operating wavelength. Furthermore, the relative dielectric constant of gold can be demonstrated by Drude-Lorentz model, which is expressed as follows[28]

$$\varepsilon(\omega)=\varepsilon_1+\mathrm{i}\varepsilon_2=\varepsilon_\infty-\frac{\omega_\mathrm{p}^2}{\omega(\omega+\mathrm{i}\omega_\mathrm{c})} \tag{2}$$

where $\varepsilon_\infty=9.75$ is the permittivity of gold at high frequencies, $\omega_\mathrm{p}=1.36\times10^{16}$ is the plasma frequency of gold, and $\omega_\mathrm{c}=1.45\times10^{14}$ is the scattering frequency of electrons, and ω is the angular frequency of the incident light.

In order to prevent the light reflects from the PCF boundary, an artificial boundary condition known as the Perfectly Matched Layer (PML)[29] is added to absorb the radiation energy at the outermost layer. SPR sensor is based on the coupling between the core mode and the plasmonic mode, a loss peak occurs at resonance wavelength. The coupling strength between the fiber core mode and the plasmonic mode is described by the confinement loss of the core mode, which is expressed as[30]

$$\alpha_\mathrm{loss}=8.686\times\frac{2\pi}{\lambda}\mathrm{Im}(n_\mathrm{eff})\times10^4 \tag{3}$$

where α_loss represents the confinement loss, $\mathrm{Im}(n_\mathrm{eff})$ is the imaginary part of the complex effective refractive index.

2 Results and discussion

Fig. 2 shows the relationship between the real part of the effective refractive index of core mode and plasmonic mode and the variation of confinement loss at a wavelength ranging from 1 800 nm to 2 300 nm at RI =1.2, in which the green curve stands for core mode, while the black curve represents the plasmonic mode.

Meanwhile, the relationship between the confinement loss of the core mode and wavelength is represented by the red curve. As shown in Fig. 2, when the real part of the effective refractive index of the core mode and the plasmonic mode are equal, a strong SPR effect can be observed with a prominent peak in the loss spectrum. In other words, a maximum energy transfers from the core mode to the plasmonic mode at the resonance wavelength.

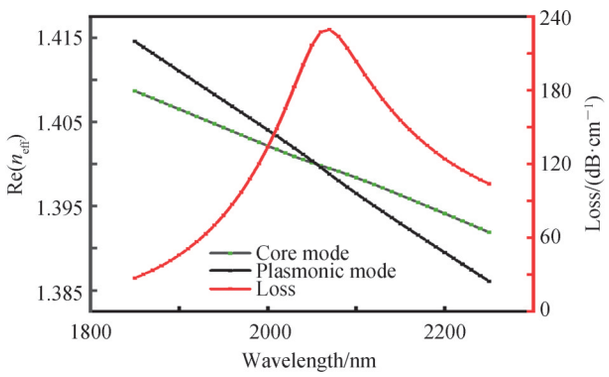

Fig. 2 Real part of effective refractive index (left axis) and confinement loss (right axis) of core mode and plasmonic mode

Fig. 3 shows the energy transfer process between core and plasmonic mode when the wavelength changes from 1 800 nm to 2 300 nm. As it can be seen from the figure, when the wavelength is away from the optimal phase matching point, most of the energy is concentrated in the core, while only a small portion of the energy leaks into the sensing interface. Obviously, the maximum energy transfers at the resonant wavelength, which is caused by the phase matching condition of core mode and plasmonic mode.

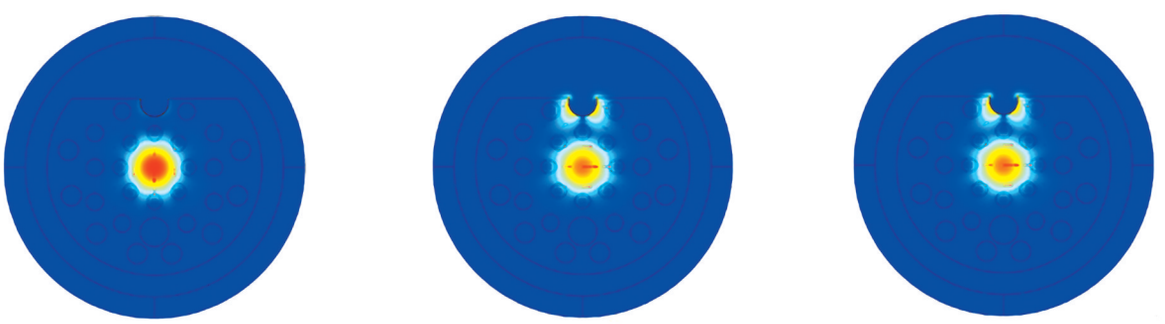

Fig. 3 The distribution of the energy of the core mode and the plasmonic mode at different wavelength

In order to optimize the sensing performance, the air holes radii, the pitch and gold film thickness were investigated separately. The refractive index of the analyte is fixed at 1.2 and the structural parameters of the PCF are calculated by keeping the rest of the structural parameters constant. The initial structural parameters r_1, r_2, r_3, r_s of the PCF are 0.5 μm, 0.6 μm, 0.7 μm and 1 μm, respectively. The innermost air hole pitch is 2.4 μm and the thickness of the gold film is 50 nm. It is worth noting that the variation of air hole diameter affects the coupling intensity and phase matching condition of core mode and plasmonic mode, thereby also affecting the energy conversion between them.

It can be seen from Fig. 4(a) that the resonance peak gradually decreases from 229.43 dB/cm to 203.49 dB/cm as r_1 changes from 0.5 μm to 0.54 μm, and the resonance wavelength shifts from 2 070 nm to a longer wavelength of 2 150 nm. This can be attributed to the fact that more energy is confined to the core when r_1 changes from 0.5 μm to 0.54 μm, which affects the coupling between the core mode and the plasmonic mode. Fig. 4(b) describes the confinement loss decrease when radius r_2 changes from 0.6 μm to 0.8 μm, and the corresponding blue shift occurs with the resonance peaks moving toward a shorter wavelength from 2 100 nm to 1 650 nm over the process. The reason is that the increase of r_2 will increase the refractive index difference between the plasmonic mode and core mode, which will affect the coupling between them. Therefore, with the

increase of r_2, the shorter wavelength can excite the plasmonic mode, resulting in the phenomenon of wavelength blue shift in the loss spectrum.

Fig. 4(c) describes the relationship between the confinement loss and the radius r_3. As can be seen from the figure, the variation of r_3 has almost no effect on the resonance wavelength and the confinement loss, which means the air hole r_3 has a slight impact on the coupling between the core mode and the plasmonic mode. So the precision requirement of the radius r_3 is low and therefore the fabrication difficulty of the sensor can be greatly reduced. Fig. 4(d) shows the effect of the different open-ring channel radii r_s on the confinement loss of the core mode. It can be seen that the confinement loss reduces from 229.43 dB/cm to 54.21 dB/cm as r_s increases slightly from 1 μm to 1.2 μm and the resonance wavelength decreases from 2 070 nm to 1 550 nm. Therefore, the performance of the proposed sensor can be optimized by adjusting the size of the open-ring channel. In this case, we set r_1=0.5 μm, r_2=0.6 μm, r_2=0.7 μm, and r_s=1 μm, respectively, for the proposed sensor.

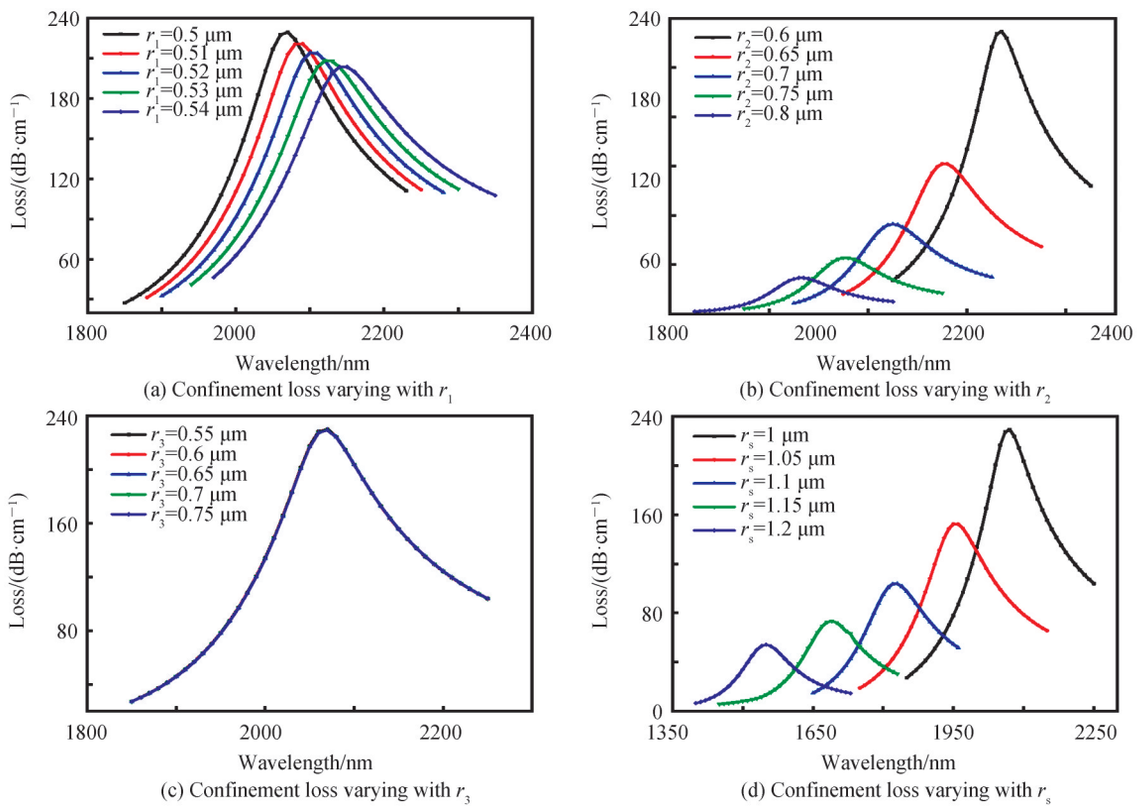

Fig. 4 The confinement loss affected by changing the radii of the air holes and the open-ring

Fig. 5(a) depicts the variation of the confinement loss of the proposed sensor with different pitches ranging from 2.4 μm to 2.56 μm. It can be seen that when Λ increases, the resonance wavelength gradually decreasing from 2 070 nm to 1 870 nm with the resonance peak decreases from 229.40 dB/cm to 96.76 dB/cm. The reason is that the change of Λ has an impact on the refractive index of core mode and plasmonic mode, which in turn affects the phase matching condition and energy coupling between them. Meanwhile, if the pitch is too large, it will prevent the concentration of the energy in the core. Totally, the pitch of 3 μm is selected to prevent the gap from increasing.

The thickness of gold film plays a vital role in the sensing performance. If the gold film is too thick, the electric field can not penetrate the gold film, which will reduce the sensitivity of the proposed sensor. While if the gold film is too thin, the plasmonic wave will be strongly suppressed due to radiation damping. Therefore, the thickness of gold film can significantly affect the coupling between the core mode and the plasmonic mode. Fig. 5(b) exhibits the loss spectra variation as the thickness of gold film ranges from 40 nm to 60 nm. As shown in Fig. 5(b), the reduction of the confinement loss and the blue shift appears as the thickness of the gold film increasing. A similar phenomenon was also noted in the paper[31]. Therefore, the sensitivity of the sensor can be

improved by optimizing the thickness of the gold film.

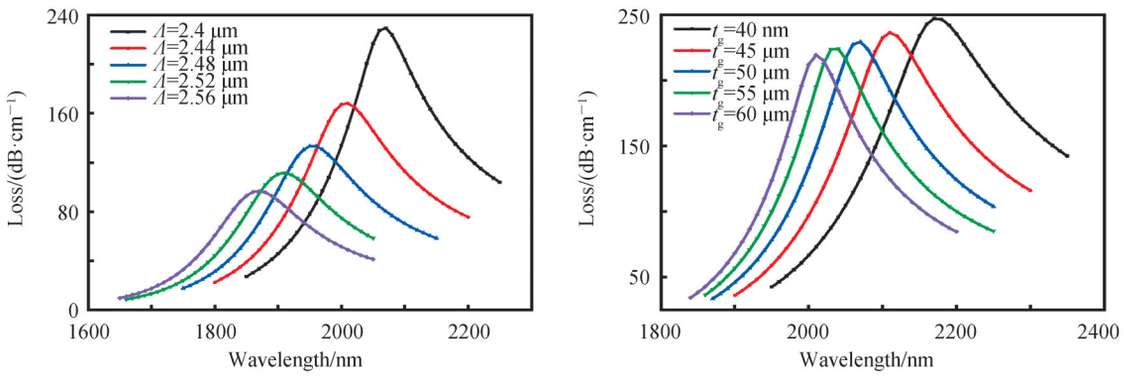

(a) Variations of loss spectra with the changes of Λ (b) Variations of loss spectra with the changes of t_g

Fig. 5 The confinement loss of the proposed sensor varies with Λ and t_g

The amplitude sensitivity is a critical parameter for evaluating the quality of the proposed sensor, and it is defined by the following equation[32]

$$S_A(\lambda)=\frac{1}{\alpha(\lambda,n_a)}\frac{\partial\alpha(\lambda,n_a)}{\partial n_a}\ (\mathrm{RIU}^{-1}) \tag{4}$$

where $\partial\alpha(\lambda,n_a)$ represents the difference of the confinement loss of the adjacent analyte RI, $\alpha(\lambda,n_a)$ denotes the overall confinement loss, and ∂n_a represents difference of the analyte RI.

The resonance wavelength is used to detect the refractive index of the analyte, which means the analyte has a significant effect on the coupling intensity between the core mode and the plasmonic mode. The wavelength dependence of the loss spectra and the amplitude sensitivity of the sensor for analytes RI ranging from 1.18 to 1.30 has been shown in Fig. 6(a) and Fig. 6(b), respectively. The resonance wavelength shifts to a longer wavelength and the peak of the confinement loss also increases gradually when the analyte RI increases from 1.18 to 1.30. This can be attributed to the incomplete coupling between the core mode and the plasmonic mode. As shown in Fig. 6(a), with the RI increasing, the confinement loss increases from 209.98 dB/cm to 579.23 dB/cm. We can notice that the maximum amplitude sensitivity is 68.13 RIU^{-1} from Fig. 6(b).

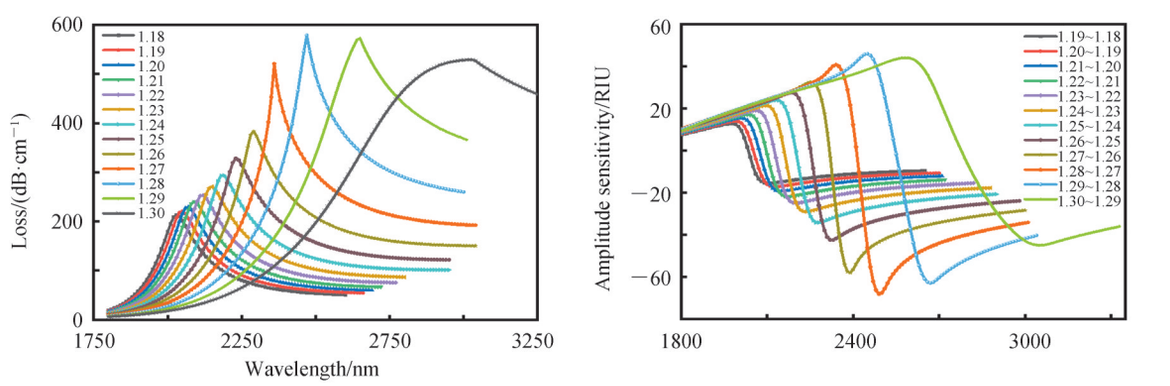

(a) Variations of loss spectra with the changes of RI (b) Variations of amplitude sensitivity with the changes of RI

Fig. 6 The increase of the confinement loss and amplitude sensitivity varies with wavelength for analyte RI from 1.18 to 1.3

Fig. 7 illustrates the fitted curve of the resonance wavelength with the analyte RI changing from 1.18 to 1.30. The inserted table shows the results of the polynomial fitting, the slope of the fitted curve represents the sensitivity of the proposed sensor. The adjusted R-square value of the fitting curve is 0.995 08, which means a high agreement of fitting. It also can be seen that the resonant point moves to longer wavelengths as the analyte RI increases, with a maximum spectral sensitivity of 388 00 nm/RIU at the analyte RI of 1.30.

The spectral sensitivity has equal significance to the amplitude sensitivity at estimating the performance of

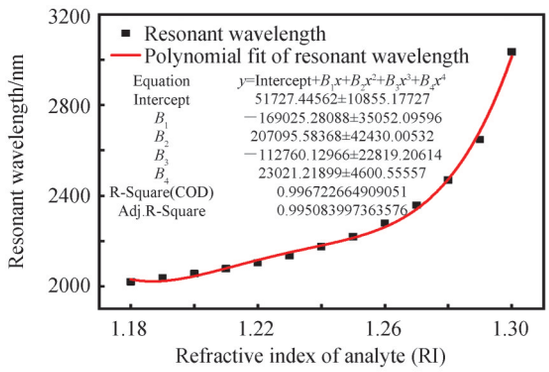

Fig. 7 The resonance wavelength varies with analyte RI from 1.18 to 1.30

the PCF sensor. The spectral sensitivity is defined by the following equation[33]

$$S(\lambda)=\frac{\Delta\lambda_{\text{peak}}}{\Delta n_{\text{a}}} \tag{5}$$

where $\Delta\lambda_{\text{peak}}$ represents the difference of the adjacent resonance wavelength.

In addition to the spectral and amplitude sensitivities, the resolution is a critical parameter of the proposed sensor. The resolution is expressed as[34]

$$R=\frac{\Delta n_{\text{a}}\cdot\Delta\lambda_{\text{min}}}{\Delta\lambda_{\text{peak}}} \tag{6}$$

where $\Delta\lambda_{\text{min}}$ is the minimum spectral resolution. A high resolution of 2.37×10^{-6} RIU can be gained at 1.30 in the proposed structure as shown in Table 1.

Table 1 shows the performance of the proposed sensor compared to previous sensors. It can be seen that the sensor proposed in this work has the advantage of higher refractive index detection. Meanwhile, the detection range of the proposed sensor is wider than that of the previous sensor.

Table 1 Comparison of the proposed sensor with previous designs

Structure	RI range	Max sensitivity / (nm•RIU^{-1})	Max resolution	Year	Ref.
D-shaped	1.23～1.29	5 500	7.69×10^{-6}	2017	[19]
Dual-shaped	1.27～1.32	13 500	7.41×10^{-6}	2018	[18]
D-shaped	1.20～1.29	11 055	9.05×10^{-6}	2019	[20]
D-shaped	1.19～1.29	10 700	----	2019	[17]
Microchannel	1.20～1.33	12 000	8.3×10^{-6}	2020	[16]
D-shaped	1.18～1.30	38 800	2.37×10^{-6}	2022	This work

3 Conclusion

In this work, a novel D-shaped PCF sensor based on SPR effect is proposed and numerically investigated. Unlike conventional D-shaped structures, the SPR effect is excited by coating in the open-ring channel with a thin gold film, which can enhance the resonance effect and improve the spectral sensitivity of proposed sensor. In addition, the usage of this channel reduces the coating area of gold film. This makes the fabrication process more simplified and cost-effective. Simulation results show that the sensor can detect low refractive indexes ranging from 1.18 to 1.30 with the highest spectral sensitivity and resolution of 38 800 nm/RIU and 2.37×10^{-6} RIU. Due to the low refractive index sensing range and the simple compact fiber design, the proposed SPR sensor could be a competitive candidate in low refractive index detection.

References

[1] CHU Suoda, NAKKEERAN K, ABOBAKER A, et al. Design and analysis of surface-plasmon-resonance-based photonic quasi-crystal fiber biosensor for high-refractive-index liquid analytes[J]. IEEE Journal of Selected Topics in Quantum Electronics, 2019, 25(2): 1-9.

[2] GOODRICH T, LEE H, CORN R. Direct detection of genomic DNA by enzymatically amplified SPR imaging measurements of RNA microarrays[J]. Journal of the American Chemical Society, 2004, 126(13): 4086-4087.
[3] OSÓRIO J, HAYASHI J, ESPINEL Y, et al. Photonic-crystal fiber-based pressure sensor for dual environment monitoring[J]. Applied Optics, 2014, 53(17): 3668-3672.
[4] CAUCHETEUR C, LOYEZ M, WATTIEZ R, et al. Evaluation of gold layer configuration for plasmonic fiber grating biosensors[J]. Optics Express, 2018, 26(18): 24154-24163.
[5] LAM W, WONG Chilok, ZHANG Yuanting, et al. A surface plasmon resonance system for the measurement of glucose in aqueous solution[J]. Sensors and Actuators B: Chemical, 2005, 105(2): 138-143.
[6] KRETSCHMANN E, RAETHER H. Notizen: radiative decay of non radiative surface plasmons excited by light[J]. Zeitschrift Für Naturforschung A, 1968, 23(12): 2135-2136.
[7] MITTAL S, SHARMA T, TIWARI M. Surface plasmon resonance based photonic crystal fiber biosensors: a review[J]. Materials Today: Proceedings, 2021, 43(17): 3071-3074.
[8] DASH J, JHA R. SPR Biosensor based on polymer PCF coated with conducting metal oxide[J]. IEEE Photonics Technology Letters, 2014, 26(6): 595-598.
[9] LIU Chao, YANG Lin, SU Weiquan, et al. Numerical analysis of a photonic crystal fiber based on a surface plasmon resonance sensor with an annular analyte channel[J]. Optics Communications, 2017, 382: 162-166.
[10] ZHAO Jing, CAO Shaoqing, LIAO Changrui, et al. Surface plasmon resonance refractive sensor based on silver-coated side-polished fiber[J]. Sensors and Actuators B: Chemical, 2016, 230: 206-211.
[11] HU Dorajuanjuan, HO Hopui. Recent advances in plasmonic photonic crystal fibers: design, fabrication and applications [J]. Advances in Optics and Photonics, 2017, 9(2): 257-314.
[12] RIFAT A, AHMED R, YETISEN A, et al. Photonic crystal fiber based plasmonic sensors[J]. Sensors & Actuators B Chemical, 2017, 243: 311-325.
[13] LUAN Nannan, WANG Ran, LV Wenhua, et al. Surface plasmon resonance sensor based on D-shaped microstructured optical fiber with hollow core[J]. Optics Express, 2015, 23(7): 8576-8582.
[14] AN Guowen, HAO Xiaopeng, LI Shuguang, et al. D-shaped photonic crystal fiber refractive index sensor based on surface plasmon resonance[J]. Applied Optics, 2017, 56(24): 6988-6992.
[15] SINGH S, PRAJAPATI Y. Highly sensitive refractive index sensor based on D-shaped PCF with gold-graphene layers on the polished surface[J]. Applied Physics A, 2019, 125(6): 437.
[16] WANG Jianshuai, PEI Li, WANG Ji, et al. Surface plasmon resonance sensor for low refractive index detection based on microstructured fiber[J]. Journal of the Optical Society of America B, 2019, 36(11): 3104-3110.
[17] YANG Zhao, XIA Li, LI Chen, et al. A surface plasmon resonance sensor based on concave-shaped photonic crystal fiber for low refractive index detection[J]. Optics Communications, 2019, 430: 195-203.
[18] WANG Famei, LIU Chao, SUN Zhijie, et al. A highly sensitive SPR sensors based on two parallel PCFs for low refractive index detection[J]. IEEE Photonics Journal, 2018, 10(4): 7104010.
[19] LIU Chao, YANG Lin, LU Xili, et al. Mid-infrared surface plasmon resonance sensor based on photonic crystal fibers [J]. Optics Express, 2017, 25(13): 14227-14237.
[20] CHEN Xin, XIA Li, LI Chen. Surface plasmon resonance sensor based on a novel D-shaped photonic crystal fiber for low refractive index detection[J]. IEEE Photonics Journal, 2018, 10(1): 6800709.
[21] DIPIPPO W, LEE B, PARK K. Design analysis of doped-silicon surface plasmon resonance immunosensors in mid-infrared range[J]. Optics Express, 2010, 18(18): 19396-19406.
[22] SACHET E, LOSEGO M, GUSKE J, et al. Mid-infrared surface plasmon resonance in zinc oxide semiconductor thin films[J]. Applied Physics Letters, 2013, 102(5): 051111.
[23] RODRIGO D, LIMAJ O, JANNER D, et al. Mid-infrared plasmonic biosensing with graphene[J]. Science, 2015, 349 (6244): 165-168.
[24] AMOUZAD M, CHOW D, SANDOGHCHI S, et al. Challenges and solutions in fabrication of silica-based photouonic crystal fibers: an experimental study[J]. Fiber and Integrated Optics, 2014, 33(1-2): 85-104.
[25] CHEN Yuzhi, XIE Qingli, LI Xuejin, et al. Experimental realization of D-shaped photonic crystal fiber SPR sensor[J]. Journal of Physics D: Applied Physics, 2017, 50(2): 025101.
[26] MALINSKY P, SLEPIKA P, HNATOWICZ V, et al. Early stages of growth of gold layers sputter deposited on glass and silicon substrates[J]. Nanoscale Research Letters, 2012, 7: 241.
[27] AKOWUAH E, GORMAN T, ADEMGIL H, et al. Numerical analysis of a photonic crystal fiber for biosensing applications[J]. IEEE Journal of Quantum Electronics, 2012, 48(11): 1403-1410.
[28] JOHNSON P, CHRISTY R. Optical constants of the noble metals[J]. Physical Review B, 1972, 6(12): 4370-4379.
[29] BERENGER J. A perfectly matched layer for the absorption of electromagnetic waves[J]. Journal of Computational Physics, 1994, 114(2): 185-200.

[30] SHUAI Binbin, XIA Li, ZHANG Yating, et al. A multi-core holey fiber based plasmonic sensor with large detection range and high linearity[J]. Optics Express, 2012, 20(6): 5974-5986.
[31] XUE Jianrong, LI Shuguang, XIAO Yuzhe, et al. Polarization filter characters of the gold-coated and the liquid filled photonic crystal fiber based on surface plasmon resonance[J]. Optics Express, 2013, 21(11): 13733-13740.
[32] LIU Min, YANG Xu, SHUM Ping, et al. High-sensitivity birefringent and single-layer coating photonic crystal fiber biosensor based on surface plasmon resonance[J]. Applied Optics, 2018, 57(8): 1883-1886.
[33] HASSANI A, SKOROBOGATIY M. Photonic crystal fiber-based plasmonic sensors for the detection of biolayer thickness[J]. Journal of the Optical Society of America B, 2009, 26(8): 1550-1557.
[34] HAUTAKORPI M, MATTINEN M, LUDVIGSEN H. Surface-plasmon-resonance sensor based on three-hole microstructured optical fiber[J]. Optics Express, 2008, 16(12): 8427-8432.

Design and Analysis of D-shaped Surface Plasmon Resonance Fiber Biosensor for Liquid Analytes

LIU Qingmin, HOU Shanglin, LEI Jingli
(*School of Science, Lanzhou University of Technology, Lanzhou* 730050, *China*)

Abstract: Surface Plasmon Resonance (SPR) is a prominent optical phenomenon that arises as the extent of energy transferring from photons to surface plasmon waves under appropriate conditions. In the past few years, this optical effect, owing to its high sensitivity, real-time detection, and anti-interference has already been extensively investigated and applied in medical treatment, environment monitoring, biomedical sensing and so on. Based on the principle of SPR, a novel D-shaped gold surface plasmon resonance photonic crystal fiber with one open-ring is proposed for detecting low refractive index materials has been investigated in detail. The proposed photonic crystal fiber of the simulation model is composed of three layers of air holes. The radii of air holes in the first-layer and third-layer are r_1 and r_3, respectively. While the second-layer air ring consists of air holes with two different radii, r_2 and r_s. The refractive index of air is fixed at $n_{air}=1$ and the radius of the cladding is R. A thin gold film with thickness t_g is deposited on the inner surface of the micro-opening analyte channel on the upper side, the radius and the central location of the channel are r_s and $2.5\times\Lambda-1.25\times r_s$, respectively. The fiber material is fused silica and the RI is determined by the Sellmeier equation, the relative dielectric constant of gold can be demonstrated by the Drude-Lorentz model. This paper uses the finite element method and sets the boundary conditions of the perfect matching layer for simulation. In order to investigate how the sensing performance of the proposed PCF-SPR sensor is affected by the parameters of the optical fiber, the effect of various parameters of the fiber such as air radii (r_1, r_2, r_3, r_s), air hole spacing (Λ) and the gold film (t_g) on the SPR loss spectrum have been studied separately. The simulation results show that the confinement loss decreases as r_1 increases. This can be attributed to the fact that more energy is confined to the core when r_1 increases, which affects the coupling between the core and plasmonic modes. At the same time, the confinement loss also decreases with the increase of r_2, and the corresponding blue shift occurs with the resonance peaks moving toward a shorter wavelength over the process. The reason is that the increase of r_2 will increase the refractive index difference between the plasmonic mode and core mode, which will affect the coupling between them. Therefore, with the increase of r_2, the shorter wavelength can excite the plasmonic mode, resulting in the phenomenon of wavelength blue shift in the loss spectrum. Since the air holes of the third layer are located at the outermost part of the fiber, the change of r_3 has little impact on the confinement loss, which can greatly reduce fabrication difficulty of the sensor. The pitches between the air holes are also an important factor in confinement loss, the change of Λ will influence the refractive index of core mode and plasmonic mode, which in turn affects the phase matching condition and energy coupling between them. The thickness of gold film plays a vital role in the sensing performance. If the gold film is too thick, the electric field can not penetrate the gold film, which will reduce the sensitivity of the proposed sensor. While if the gold film is too thin, the plasmonic wave will be strongly suppressed due to radiation damping. Therefore, the thickness of gold film can significantly affect the coupling between the core mode and the

plasmonic mode. After optimizing the various parameters affecting the sensing performance of the sensor, we analyse the analytes with different refractive indices. Simulation results show that the sensor operates in the near-infrared and mid-infrared region with the wavelength range of 2 020～3 036 nm in the refractive index range of the analyte of 1.18～1.30. When the refractive index of the analyte is in the range of 1.23 to 1.30, the sensor operates in the band of 2 135～3 036 nm, and the average value of spectral sensitivity is up to 11 650 nm/RIU. When the refractive index of the analyte is between 1.29 and 1.30, the sensor operates in the mid-infrared band of 2 648～3 036 nm, and the maximum spectral sensitivity and resolution are 38 800 nm/RIU and 2.37×10^{-6} RIU, respectively. The proposed sensor shows great significance in detecting low refractive indexes in near- and mid-infrared waveband, and has potential applications in biomedical sensing, water environment and humidity detection and so on.

Key words: Optical fiber sensor; Surface plasmon resonance; Finite element method; Photonic crystal fiber; Low refractive index sensor

OCIS Codes: 060.2370; 280.4788; 240.6680; 240.6690